



Atmospheric Chemistry and Physics
2020 Manuscript, Rev. May 2020

Captured Cirrus Ice Particles in High Definition

Nathan Magee*, Katie Boaggio, Samantha Staskiewicz, Aaron Lynn, Xuanyi Zhao, Nicholas Tusay, Terance Schuh, Manisha Bandamede, Lucas Bancroft, David Connelly, Kevin Hurler, Bryan Miner, and Elissa Khoudary.

*Corresponding Author: magee@tcnj.edu

Affiliations:

Boaggio: ORISE Participant at U.S. Environmental Protection Agency

Hurler: University of South Carolina

Bandamede: Ross University School of Medicine

Connelly: Cornell University

Bancroft: Universal Display Corporation

Staskiewicz: The Pennsylvania State University

Magee and others: The College of New Jersey (TCNJ)



1 **Abstract**

2 Cirrus clouds composed of small ice crystals are often the first solid matter encountered by
3 sunlight as it streams into Earth's atmosphere. A broad array of recent research has emphasized
4 that photon-particle scattering calculations are very sensitive to ice particle morphology,
5 complexity, and surface roughness. Uncertain variations in these parameters have major
6 implications for successfully parameterizing the radiative ramifications of cirrus clouds in
7 climate models. To date, characterization of the microscale details of cirrus particle morphology
8 has been limited by the particles' inaccessibility and technical difficulty in capturing imagery
9 with sufficient resolution. Results from a new experimental system achieve much higher
10 resolution images of cirrus ice particles than existing airborne particle imaging systems. The
11 novel system (Ice Cryo-Encapsulation by Balloon, ICE-Ball) employs a balloon-borne payload
12 with environmental sensors and hermetically-sealed cryo-encapsulation cells. The payload
13 captures ice particles from cirrus clouds, seals them, and returns them via parachute for vapor-
14 locked transfer onto a cryo-scanning electron microscopy stage (cryo-SEM). From 2016-2019,
15 the ICE-Ball system has successfully yielded high resolution particle images on nine cirrus-
16 penetrating flights. On several flights, including one highlighted here in detail, thousands of
17 cirrus particles were retrieved and imaged, revealing unanticipated particle morphologies,
18 extensive habit heterogeneity, multiple scales of mesoscale roughening, a wide array of
19 embedded aerosol particles, and even greater complexity than expected.
20



21 1. Introduction

22 Understanding of cirrus cloud microphysics has advanced dramatically in the past several
23 decades thanks to continual technical innovations in satellite remote sensing, in-situ aircraft
24 measurements, sophisticated laboratory experiments, and modeling that incorporates this new
25 wealth of data. In combination, the au courant picture of cirrus clouds has emerged: a highly
26 complex system that results in a vast array of cirrus formations, varying in time and location
27 through interdependent mechanisms of microphysics, chemistry, dynamics, and radiation (e.g.
28 Heymsfield et al. 2017). While the net magnitude of cirrus radiative forcing is clearly not as
29 large as thick low-altitude clouds, an intricate picture of climate impacts from cirrus is coming
30 into focus. It now seems clear that both the sign (positive or negative) and strength of cirrus
31 radiative forcings and feedbacks depend on variables that can change with a wide array of
32 parameters: geography, season, time of day, dynamical setting, and the concentrations, shapes,
33 sizes, and textures of the cirrus ice particles themselves (e.g. Burkhardt and Kärcher, 2011;
34 Harrington et al. 2009; Järvinen 2018b, Yi et al. 2016). Furthermore, many of these factors may
35 be changing markedly over time, as contrail-induced cirrus and changing temperature, humidity,
36 aerosol in the high troposphere are affected by evolving anthropogenic influences (Randel and
37 Jensen, 2013; Kärcher et al. 2018, Zhang et al. 2019). Undoubtedly, a sophisticated, high-
38 resolution understanding of cirrus is critical to accurately model the impacts to global and
39 regional climate.

40 Satellite-derived measurements of cirrus properties have become vastly more
41 sophisticated with the advent of increased spatial and temporal resolution, a broader array of
42 spectral channels, specialized detectors, and advances in scattering theory (e.g. Yang 2008;
43 Baum 2011; Sun 2011; Mauno 2011; Yang 2013; Cole 2014; Tang 2017, Yang et al. 2018).
44 Where a generation ago it was challenging to even isolate the presence of cirrus clouds in much
45 satellite imagery, it is now routine to derive estimates of ice cloud optical depth, cloud top
46 temperature, cloud top height, effective particle size, and in some cases even to infer the
47 dominant particle habit and roughness of crystal surfaces (McFarlane 2008; King 2013; Cole
48 2014, Hioki et al. 2016, Saito et al. 2017). The emerging ubiquity of this sophisticated satellite
49 data and highly-developed retrieval schemes can sometimes obscure the fact that major
50 fundamental uncertainties remain regarding cirrus microphysical compositions and their
51 intertwined dynamic evolution.



52

53 Cloud particle imaging probes on research aircraft have also contributed to major leaps in
54 understanding, helping to constrain cirrus property satellite retrievals and climate modeling
55 representations (Baumgarnder et al. 2017; Lawson et al. 2019). These probes deliver particle
56 imaging and concentration measurements that yield unique insights into ice particle habits and
57 distributions in cirrus, though several significant limitations remain. The SPEC Inc. CPI probes
58 have flown for nearly 20 years and can achieve 5 μm particle optical resolutions and SPEC's 2D-
59 S stereo imaging probe yields 10 μm pixel sizes (Lawson et al. 2019). For example, CPI images
60 of cirrus ice were featured on the June 2001 cover of the Bulletin of the American
61 Meteorological Society (Connelly et al. 2007) and have contributed to many other cloud physics
62 field programs since (for complete list, see Appendix A in Lawson et al. 2019). Other recent in-
63 situ particle measurement innovations include the HOLODEC (Fugal 2004), SID3 (Ulanowski et
64 al. 2012, Järvinen et al 2018a), and PHIPS-Halo (Schnaiter 2018), with imaging resolutions on
65 the order of 5-10 microns, as well as multi-angle projections, and indirect scattering
66 measurements of particle roughness and complexity. High speed aerodynamics and concerns
67 about instrument-induced crystal shattering have produced some uncertainties regarding inferred
68 particle concentrations, size distributions, and orientations, but perhaps more importantly, the
69 limited optical resolving power means that in-situ imaging instruments are not able to determine
70 fine-scale details of crystal facet roughness or highly complex habit geometry, particularly for
71 small ice crystals. Several groups have also achieved recent in-situ measurements of cirrus
72 particles using balloon-borne instruments (Miloshevich and Heymsfield 1997; Cirisan et al.
73 2014; Kuhn and Heymsfield 2016; Wolf et al. 2018). Though this has been a relatively sparse
74 set, some slight momentum appears to be building toward exploiting advantages of this slower-
75 speed probe.

76 The synthesis that has been emerging describes cirrus clouds that are often, but not
77 always, dominated by combination of complex particle morphologies, and with crystal facets that
78 usually show high roughening and complexity at the microscale (Baum et al. 2011; Yang et al.
79 2013; Yi et al. 2013; Tang et al. 2017; Heymsfield et al. 2017; Lawson et al. 2019). Particle
80 complexity has been considered to encompass an array of potential geometric deviations away
81 from a simple hexagonal, single ice crystal: intricate polycrystalline morphological shapes,
82 aggregations of individual particles, partial sublimation of particles, post-sublimation regrowth



83 of microfacets, and inclusions of bubbles and aerosol particles (Ulanowski et al. 2012; Schnaiter
84 et al. 2016; Voitlander et al. 2018). Even where crystals may present mainly planar facet
85 surfaces, these surfaces are often characterized by regular or irregular patterns of roughening at
86 multiple scales. All aspects of increased complexity and roughening have been shown to smooth
87 and dampen the characteristic peaks in the scattering phase function of hexagonal ice crystals
88 (van Diedenhoven 2014). The angular integral of the phase function yields the asymmetry
89 parameter, which has been broadly applied as an indicator of net radiative impact of underlying
90 particle microphysics (Baran 2015). With mesoscopic crystal roughness and complexity
91 contributing to less total forward scattering, the asymmetry parameter and net downwelling
92 radiation is reduced (e.g. Yang and Liou 1998; Um and McFarquhar 2011, van Diedenhoven et
93 al. 2013). The calculated impacts on cirrus cloud radiative effect are shown to be
94 climatologically significant compared to assumptions that cirrus composed of less complex
95 crystals (Yang et al. 2013; Järvinen et al. 2018b). Furthermore, beyond questions of particle
96 morphology and radiative balances, major uncertainties around cirrus cloud evolution remain
97 regarding particle nucleation pathways and the interconnected roles of aerosol chemistry, high-
98 altitude humidity, and the subtle dynamics of vertical motion and turbulent eddies in cirrus.

99 **2. ICE-Ball in-Situ Capture Methods**

100 **2.1 ICE-Ball System**

101 The ICE-Ball experiment has been designed, refined, and implemented from 2014-2018. The
102 basic system consists of a ~2 kg payload (“Crystal Catcher”) carried aloft by a 300 g latex
103 weather balloon. The payload components are enclosed in a mylar-wrapped Styrofoam cube
104 (Fig. 1) to prevent electronics from freezing and to comply with FAA regulations for weight,
105 density, and visibility. Figure 1 shows authors Tusay, Lynn, and Zhao holding ICE-Ball, along
106 with a cross-section diagram of the cryo-collection and preservation mechanism. The instrument
107 suite consists of standard balloon sonde sensors (pressure, temperature, and dewpoint), and also
108 includes HD video (GoPro Session) and dual real-time GPS position tracking (SPOT and
109 GreenAlp). The cryo-capture vessel and ice encapsulation cell comprise the novel ice particle
110 capture and preservation mechanism. Several versions of this mechanism have been employed,
111 but in each case, it has consisted of a vacuum-insulated stainless steel vessel (250 ml volume)
112 filled with crushed dry ice and containing a custom-machined sweep tube and ice encapsulation
113 cell. The sweep tube extends slightly above the top of the payload, and passively collects



114 particles in its path due to the upward motion of the balloon (~5 m/s). When the collection
115 aperture is open, the particles settle to the bottom of the collection tube and are gravitationally
116 deposited in the ice encapsulation cell, which is nestled in the surrounding dry ice. The
117 encapsulation cell interior diameter is 7 mm, and has an open volume of 0.2 cm³.

118 During ascent, the balloon is ~20 ft above the payload and does not appear to affect
119 particle concentrations impacting the top of the payload. Several sweep tube geometries and
120 opening sizes have been tested (from 0.5 to 5 cm²), but in each case, streamline modeling and
121 sample analyses suggest that collection efficiencies are high for particles larger than 50 microns
122 and decrease at smaller sizes. Cirrus cloud conditions and the in-flight collection operation is
123 recorded via the go-Pro video. Cirrus particles are routinely observed passing the camera, and
124 either 22° halos and/or circumzenith arcs can often be observed on the video record of each
125 successful flight.

126 **2.2 Ice Crystal Preservation**

127 The apertures to the cryo-vessels' sweep-tubes can be opened and closed using a rotational servo
128 motor that is driven by an Arduino microprocessor (a previous version used robotic clamshell
129 seals, as seen in Supplement2 video). The Arduino is programmed to open the path to each
130 collection vessel individually at cirrus altitudes that are prescribed before each launch.
131 Immediately after transiting the prescribed collection zone(s), the apertures are closed and a
132 magnetic sphere is dropped down the collection tube to seal the collected crystals in the small-
133 volume encapsulation cell (see Fig. 1b). This onboard preservation system has been tested to
134 preserve collected crystals in pristine condition for approximately 6 hours, which usually
135 provides ample time for recovery. Upon ICE-Ball landing and recovery, the small volume
136 encapsulation cell is hermetically double-sealed and stored in dry ice to ensure that crystals are
137 preserved as pristinely as possible. After returning to the lab, the sealed ice-crystal samples can
138 also be stored in liquid nitrogen for medium-term storage of up to several days prior to transfer
139 and imaging in the cryo-SEM.

140 **2.3 Flight Record**

141 Intensive field campaigns were conducted during June and July of 2016-2019, consisting of 5-10
142 flights per campaign. In order to proceed with mission launch, the following conditions were
143 required: 1) greater than 50% projected cirrus coverage at the time of launch, 2) horizontal wind
144 speeds (trajectory mean) less than 60 kt, 3) modeled trajectory allowing for a safe launch zone



145 and an open landing zone within a 1 hour drive of TCNJ, 4) FAA/ATC approval, requiring flight
146 plan filing 24 hours prior to launch. Conditions that prevented launches on particular days
147 mainly included high wind speeds at altitude, and clear skies or poorly predicted cirrus cloud
148 coverage. During mid-Atlantic summer, high altitude mean wind speeds meet the speed 60 kt
149 maximum launch threshold approximately 60% of the time; regional climatological proximity to
150 the jetstream often results in prohibitively high winds in the upper troposphere during other
151 seasons. High wind speeds result in a longer flight trajectory (50 kt mean wind yields ~ 50 mile
152 flight), degrading landing zone accuracy (nominal landing position prediction error radius of
153 10% of the trajectory length). Longer flight paths also require additional drive time and increase
154 the risk of landing in an inaccessible or unsafe location (e.g. Atlantic Ocean, Military Base,
155 Airport, or Interstate). In the summertime mid-Atlantic region, cirrus coverage is approximately
156 20%. The accuracy of cirrus coverage forecasts by NCEP operation weather models (GFS,
157 NAM, and HRRR) were found to be a significant challenge to launch planning. Models of high-
158 cloud forecasts appear not to produce significant skill beyond ~48 hour lead times, though it is
159 likely that these fields have not been refined as carefully as others due to modest influence on
160 surface weather.

161 The novel experimental system has failed to recover ice crystals on more occasions than
162 it succeeded (38% crystal recovery rate). As the team gained more experience, the success rate
163 improved (65% during the final campaign), but systemic experimental challenges remain.
164 Conditions that resulted in failure to capture or recover cirrus ice crystals were somewhat varied:
165 system technical failures including premature balloon bursts and frozen electronics (6
166 occurrences); ICE-BALL landing zone (often high in a tree canopy) resulted in recovery time
167 that was too long to preserve crystals (6 times); flight trajectory missed scattered cirrus clouds (4
168 times); failure of Cryo-transfer or SEM outage (2 times). Perhaps the most difficult obstacle to
169 the further development and deployment of the experimental system is the challenge associated
170 with difficult to access landing zones. This is especially challenging in the mid-Atlantic where
171 geography results in only small pockets of public property and high fractions of tree coverage.
172 Remarkably, all 28 flights were eventually recovered, but 4 of these included instances of the
173 system caught higher than 50 feet up in a tree, which typically resulted in a complex multi-day
174 effort to retrieve.



175 **2.4. Vapor-lock transfer and cryo-SEM imaging**

176 A unique cryo-SEM imaging capability for captured samples is provided by a Hitachi SU5000
177 SEM, equipped with a Quorum 3010 Cryosystem and EDAX Octane Energy Dispersive
178 Spectroscopy (EDS). The Hitachi SU5000 employs a Schottky field emission electron gun
179 and variable pressure sample chamber. The combination of the variable-pressure FE-SEM
180 chamber with the Quorum cryosystem is a unique configuration that allows samples to be
181 transferred, held, and imaged uncoated at very low temperature (usually $\sim 160^{\circ}\text{C}$), while
182 simultaneously ensuring that excess water vapor is not deposited or removed from the sample
183 surfaces. The Quorum 3010 Cryosystem integrates a cryo-airlock that transfers a frozen
184 encapsulation cell into the SEM chamber while maintaining cryo-cooling and hermetic sealing
185 throughout the transfer process. Once the SEM chamber has been loaded with the crystal sample
186 and balanced cryo-temperature and pressure achieved, the magnetic seal is removed and imaging
187 can commence.

188 Electron beam accelerations of 2kV – 20 kV have been successfully employed with
189 Hitachi backscatter and secondary electron detectors to produce micrographs of the captured ice
190 crystals. The backscatter images in particular produce a dramatic contrast between the ice and
191 higher-density embedded aerosol particles that often include silica minerals and metal oxides.
192 The image resolutions of individual micrographs depend on multiple factors including SEM
193 beam energy, spot size, working distance, and beam scanning speed. Generally, lower
194 magnification micrographs near 100x magnification achieve resolutions of 500-1000 nm, while
195 moderate magnification images near 2000x have resolutions of 25-50 nm. Although used
196 somewhat less frequently for these samples due to limited field of view, higher magnification
197 images of 5000x or above routinely achieve 10 nm resolution. At magnification above 30kx,
198 resolution approaching 2 nm is possible in this configuration, however, this results in a very
199 small field of view without prominent ice facet features, and appears to alter the ice surface
200 unless very low beam energies are used. It is someone easier to achieve sub-5 nm resolution,
201 crisp focus and high contrast images without deforming the ice surfaces if the samples are cryo-
202 sputter coated and then imaged in high vacuum. However, this process has not been used
203 frequently because the cryo-sputtering process appears to obscure the smallest nanoscale surface
204 roughness patterns, and also complicates the prospects for using EDS to measure composition of
205 aerosol particles.



206 **3. Results: Cirrus Ice Crystal Capture**

207 Particularly with respect to detailed visualization of mesoscale roughness and complexity, the Ice
208 Cryo Encapsulation by Balloon (ICE-Ball) probe demonstrates the capability to dramatically
209 enhance knowledge of fine-scale details of cirrus ice particles. In the four successful collection
210 flights from November 2015-August 2017, small numbers (min. 3, max. 20) of intact ice crystals
211 were recovered and imaged by Cryo-SEM. In Spring 2018, the collection aperture was
212 significantly enlarged, which resulted in collection of thousands of crystals on six successful
213 flights during Spring and Summer 2018-2019. The flight on April 24, 2018 was particularly
214 successful, and provides the focus of the results presented here (Fig. 2, Fig. 3, and Table 1) due
215 to the large number of very well-preserved crystals and the synchronous alignment with well-
216 defined NASA A-Train satellite measurements.

217 The other successful recoveries also yielded significant data, including some marked differences
218 in the morphology of ice crystals captured from the high-altitude clouds. Example ice particle
219 images for these additional flights are provided in supplemental data, along with a description of
220 the synoptic context. Within this sample set, high thin in-situ cirrus (Fig. 4., Supl. 1-E and 1-G)
221 and ice particles within proximity of convection (Supl. 1-C) tended to be smaller and more
222 compact than examples collected from actively growing warm-advection cloud shields (e.g. Fig.
223 2, Fig. 3, Table 1, and Supl. 1-D).

224 **3.1 Synoptic Atmospheric Context on 4/24/2018**

225 On the morning of April 24th, 2018, a surface low pressure system was moving from the
226 Carolinas toward the Northeastern United States. Warm advection aloft generated a shield of
227 ascending air to the north and east of the low, resulting in the emergence of a large region of
228 cirrus and cirrostratus. At mid-morning over central New Jersey, this cirrus deck extended from a
229 9.3 km base to a 11.5 km cloud top, with an optical depth near 2.0 (NOAA/CIRA analysis
230 algorithms on GOES-16 data). For much of the morning, a faint 22 degree optical halo was
231 visible from the ground in the filtered sunlight, and is also clearly visible from in-flight video
232 (available in supplemental data). The ICE-Ball system was deployed at 11:05 am from near
233 Bordentown, NJ. The payload ascended at approximately 6 m/s, penetrating the ~2 km thick
234 cirrostratus near Ewing, NJ at 11:45 am. Winds at this altitude were 55 kts from the south, with a
235 cloud base temperature of -40°C and a cloud top temperature of -55°C. Video from the flight
236 payload recorded ice particles impacting ICE-Ball for approximately 7 minutes as the instrument



237 ascended through the cirrus thickness. While the 22 degree halo was clearly evident, no distinct
238 circumzenith arc was visible on this flight, which was often observed in video at altitude on other
239 ICE-Ball cirrus penetrations (for example in the Supplement 2: Flight video montage). The
240 balloon burst at 14 km altitude, and the payload descended via parachute, landing in
241 Hillsborough, NJ. Recovery occurred approximately 10 minutes after landing, and the captured
242 and sealed ice particles were transferred into the Cryo-SEM for imaging at approximately 3:00
243 pm.

244 **3.2 Multiformal and Intricate Particle Morphology**

245 Captured ice particles from 4/24/2018 and from other flights show striking morphological
246 diversity and complexity. Despite a collection mechanism that principally reveals particles from
247 near the top of a single cirrus layer, an extraordinarily wide variety of habits are apparent from
248 each single cloud penetration, including particles of nearly every cirrus habit classification that is
249 already recognized (e.g. from Bailey and Hallett, 2009) and several other discernible geometric
250 forms that have not been reported elsewhere. Among the most striking features of the particle
251 images is that every aspect of particle morphology is present in multifarious patterns. Even from
252 one section of one cirrus cloud, and among recognizable particle habits, major inhomogeneities
253 are present including wide ranges of particle size, aspect ratio, varying degrees of hollowing,
254 trigonal to hexagonal cross symmetry, broad variations in polycrystallinity, and particles that
255 range from highly sublimated to those with pristinely sharp edges and facets. Perhaps the best
256 way to appreciate this immense diversity in particle form is through the stitched mosaic
257 micrograph from 4/24/18 (Fig. 2). This mosaic of 50 lower-magnification Cryo-SEM images
258 (100x) captures the entirety of one ICE-Ball sample collection cryo-cell, with a circular inside
259 diameter of 7.0 mm. Each individual image field is 0.97mm tall x 1.27 mm wide, with a pixel
260 resolution of 992 nm. An automated multi-capture algorithm on the Hitachi SEM drove the
261 sample stage to consistent overlap with a high-quality reconstruction; only in the bottom left of
262 the mosaic is some minor mismatch apparent. The mosaic figure uses false-color to highlight
263 several particle habits (bullet rosettes, columns, and plates) that fit classic definitions of
264 morphology. In total, these distinct-habit particles number ~185 of the approximately 1600
265 individual ice particles that are distinguishable within the depth of focus visible from the top of
266 the sample. The remaining ~88% of ice particles resolved in figure 2 include the following: a)
267 complex polycrystal assemblages, often not radiating outward from a single point (~75%), b)



268 highly sublimated particles where the original habit is no longer distinct (~5%), c) single bullets
269 apparently broken off from rosettes (~5%), and d) compact particles with convoluted facets
270 (~1%). Comparable convoluted crystal forms do not appear to have been reported in the
271 literature and these particles are labeled as “outré polyhedra”. Measurements of cross section
272 area, ellipse-fit dimensions, solidity, and aspect ratio for these particles are provided in Table 1.
273 In this sample, the top focal plane reveals only the first several layers of collected crystals. The
274 full sample collection was accumulated 4 mm deep with an estimated ~35 particle/mm packing,
275 and thus estimates that approximately 200,000 individual cirrus ice particles were captured and
276 preserved in this sample alone.

277 **3.3 Surface Texture Roughness with Multiple Scales and Patterning**

278 Higher resolution images reveal the topography and textures of crystal facets and edges in
279 greater detail. Even in the most pristinely faceted crystals that show no evidence of sublimation,
280 meso-scale texture on the facet surfaces is nearly always apparent at some scale. On some
281 particles and facets, the roughening is dramatically apparent, with micron-scale features in depth
282 and wavelength. On other facets, the roughness is significantly more subtle, with dominant
283 patterning at scales less than 200 nm. In addition, some particles show roughness at multiple
284 scales simultaneously. While particle complexity and micron-scale roughness are apparent at
285 100x, resolving the smaller-scale surface textures requires micrograph resolutions of at least 100
286 nm and carefully tuned contrast. Figure 3 highlights varying degrees of surface roughness in six-
287 panel micrographs from April 24th, ranging from 250x to 20000x magnification. Panel A. and B.
288 show examples of the outré polyhedron designation; panel c. demonstrates the open scrolling
289 seen on a subset of particle facets. It is straightforward to achieve crisp image focus (both
290 secondary and backscatter) from magnifications of 10x to 5000x in the Hitachi SU5000 with
291 Quorum cryo-stage, operating at 10-20 Pa in variable pressure mode with stage temperature near
292 -160°C. Beyond 5000x magnification, crisp focus in variable pressure mode is harder to achieve,
293 particularly while balancing with a goal of avoiding high beam currents which can induce slight
294 in-situ sublimation at higher beam energy, density, and exposure times. Nevertheless, at -160°C
295 and medium beam density, ice particles have extremely low vapor pressure, and even smaller
296 vapor pressure gradients, such that they can be imaged for hours without noticeable changes in
297 shape or surface texture at the nm scale. Particles can even be re-sealed while under cryo-



298 vacuum and removed from the cryo-stage for short-term storage in low-temperature freezers or
299 liquid nitrogen immersion.

300 **3.4 Ice-embedded Aerosols and Particulates**

301 All ice crystal retrievals (and those that did not capture ice) have also collected numerous aerosol
302 particulates. Although it has not yet been tractable to measure a large fraction of these scavenged
303 and embedded particulates several dozen have been measured by Energy Dispersive
304 Spectroscopy (EDAX-EDS), revealing wide-ranging compositions that include mineral dust,
305 soot, fly-ash, and confirming previous reports of biogenic aerosol (e.g. Pratt et al. 2009). Figure
306 4 includes three examples of aerosols collected by ICE-Ball, along with EDS spectra of a fly ash
307 aerosol (Fig. 4b) and iron-rich aerosol particle (Fig. 4c) adhering in the shallow hollow of a
308 trigonal single crystal. The particulates are highly variable in size, concentration, and
309 composition, with particles on the surface of crystals, and many additional particles revealed in
310 the residual samples left by a post-imaging sublimation process in the SEM. As the complex ice
311 particles sublimate, the embedded aerosol particulates collapse and coagulate with neighboring
312 particles, and leave a cohesive collection of mixed aerosol particulates near the center of the
313 original ice crystal. This sublimation-chemical coagulation process may point to a potentially
314 important cloud-processing effect that could occur during cirrus particle sublimation, possibly
315 enhancing the ice-nucleating efficiency of the original particulates (Mahrt et al. 2019). As
316 aerosols of different origin and chemistry conjoin in close proximity under intense sunlight, the
317 post-sublimation ice particle residuals may serve as an unexpected chemical mixing-pot, altering
318 the course of their impact on subsequent cirrus formation. Ice particle residuals have been
319 captured during several previous aircraft field campaigns, but these techniques are primarily
320 restricted to small ice particles (less than 75 μm) and typically can not provide morphological
321 imaging of aerosol (Czico and Froyd 2014). With additional flights and increased sampling
322 statistics, the ICE-Ball aerosol collection technique promises to provide an important
323 complement to research on the origin and processing pathways of particulates in cirrus clouds
324 within the high troposphere and across the tropopause.

325

326 **4. Conclusions**

327 Perhaps unsurprisingly, this higher-resolution view of the ice particle constituents of cirrus
328 reveal new and unanticipated complexities compared to existing laboratory, aircraft, and satellite



329 measurements. The measurements from ICE-Ball do not contradict laboratory measurements
330 (Bailey and Hallett 2004) nor do they really dispute the first-order habit diagrams that encompass
331 cirrus temperatures (Bailey and Hallett 2010). Many of the recent particle observations based on
332 in-situ imaging from aircraft field campaigns and analysis are also largely corroborated (e.g.
333 Fridlind et al. 2016, van Diedenhoven et al. 2016a and 2016b, and Lawson et al. 2019).
334 Nevertheless, present results heighten the appreciation of cirrus particle complexity in four broad
335 categories:

336 **4.1 Immense whole-particle habit heterogeneity within single cirrus clouds**

337 In all cases where multiple crystals were recovered, we observe that the synoptically-forced
338 cirrus clouds contain a multiplicity of recognizable habit types, even within the same region of
339 the cloud, and often existing outside of their expected habit temperature and pressure regime. In
340 addition (and in concurrence with Fridlind et al. 2016 and Lawson et al. 2019), we also find that
341 a high fraction of particles could be classified as “irregular”, in that they do not fit within an
342 established habit category. The high-resolution images demonstrate that these non-categorized
343 particles are mainly divided between a) highly-sublimated forms where the original habit is no
344 longer recognizable and especially b) sharp-edged, faceted particles with complex
345 polycrystalline morphology that does not neatly fit in established habit categories. In most
346 instances, these polycrystalline assemblages can not truly be described as plate rosettes, because
347 the multiple crystals often do not radiate outward from a single focus, and they also frequently
348 contain plate-like and columnar crystal forms in a single particle. Furthermore, all of the sharp-
349 edged, and neatly-faceted crystals with no hint of sublimation commonly occur in direct
350 intermixture with highly sublimated particles. Due to our inherent sampling bias, this observation
351 may only be particularly apparent at the upper edges of cirrus clouds where entrainment mixing
352 is prevalent. Nevertheless, this upper-edge region is also of particular radiative importance,
353 especially in optically thicker cirrus. Despite this diverse morphology within each single cloud,
354 the set of 9 flight samples also reveals significant patterns of particle variations that appear to be
355 linked to the dynamical and air-mass characteristics of the cloud. For example, degree of aerosol
356 loading, average particle size, mean aspect ratio, in-cloud particle concentration, and degree of
357 polycrystallinity are fairly consistent within each single collection. On one flight, several sets of
358 collected particles appear as an aggregated chain (Fig. 5c; Supplement 1G.); this cirrus cloud was



359 not near active convection, but the frontal cirrus original may have derived from modest
360 convection several hours prior to collection.

361 **4.2 Widespread non-hexagonal faceting, hollowing, and scrolls**

362 In addition to unexpectedly convoluted whole-particles, captured ice particle sub-structures and
363 facets also show a sizeable fraction of trigonal (e.g. Fig. 3b, 4b, 5a), rhomboid (Fig. 3b) and
364 other non-hexagonal symmetries. In fact, facets with hexagonal symmetry appear to be a slight
365 minority. For example, columnar single-crystals in figure 2 are shaded in yellow for trigonal or
366 other-shaped basal cross-sections (53) and green for hexagonal basal cross-section (30). Bullet
367 rosette cross sections also appear to follow similar proportions. For both bullet rosettes and
368 columnar habits in figure 2, approximately 80% of crystals demonstrate some degree of
369 hollowing. This proportion is similar, though slightly higher than reported by Schmitt and
370 Heymsfield (2007). Smith et al. (2015) also report experiments on the single-scattering impacts
371 of column hollowing, pointing out that greater hollowing extent tends to increase the asymmetry
372 parameter, but that the topographical character of the hollowing itself is also important. In
373 addition to typical center-hollowing, a small fraction (~1%) of ice particles from multiple flights
374 have prominent “scrolled” geometry (purple in Fig. 2, Fig. 5d) which has been reported in lab
375 experiments but rarely observed in the atmosphere. Figure 5b shows a set of fairly compact and
376 relatively small crystals; their unusual convoluted faceting would likely not be recognizable
377 without resolutions of 1 μm or less. A recent paper by Nelson and Swanson (2019) combine lab
378 growth experiments with adjoining-surface molecular transport kinetics to explain the
379 development of “protruding growth” features at laterally-growing ice facets that may be
380 important contributions to these secondary morphological features. This proposed mechanism
381 also highlights the role of growth and sublimation cycling in these formations, and helps to
382 explain the origins of terracing, sheaths, pockets, and trigonal growth, all of which are frequently
383 observed in ICE-Ball samples.

384 **4.3 Mesoscopic roughening at multiple scales and diverse texturing**

385 In high-magnification micrographs with resolution finer than approximately 200 nm, mesoscale
386 surface roughening on crystal facets and non-faceted sublimation surfaces is nearly always
387 apparent, but does not appear to occur at a characteristic scale-size or texture pattern in
388 individual clouds, or even on a single particle. With the smoothest, flattest facets, roughening
389 patterns may only become apparent with resolutions near or better than 200 nm combined with



390 carefully tuned contrast. In these instances, the smoothest facets show only subtle topographic
391 variations with amplitudes smaller than the wavelength of visible light (nano-scale roughening).
392 Many facets show roughness scales (amplitude and pattern wavelength) on the order of 500 μm
393 (mesoscopic roughening) and yet others reveal more dramatic roughening with scales in excess
394 of 1 μm (microscopic scale roughening). In our sample retrieval from 4/24/2018, particles in the
395 mesoscopic roughening scale range appeared most commonly. We observe that these natural
396 cirrus particles typically (but not universally) present linear roughening on prism facets and
397 radial, dendritic, or disordered roughening patterns on basal facets (Fig. 3 panels, and
398 Supplement 1). These observations of roughening are quite similar to those observed for ice
399 particles grown within environmental SEM (Magee et al. 2014; Pfalzgraff et al. 2010; Neshyba
400 et al. 2013, Butterfield et al. 2017) as well a new experimental growth chamber built specifically
401 to investigate ice surface roughening (Voigtländer et al. 2018). These observations of roughness
402 at amplitudes and patterning agree with in-situ reports of multi-scale roughness by Collier et al.
403 2016. The marked similarities in roughness seen on ICE-Ball samples and lab-grown samples
404 substantiates ESEM and other growth chamber methods as important tools for understanding
405 mesoscale roughening patterns in cirrus ice growth and sublimation, especially given their
406 unique ability to observe facets dynamically as they experience growth and sublimation cycling.

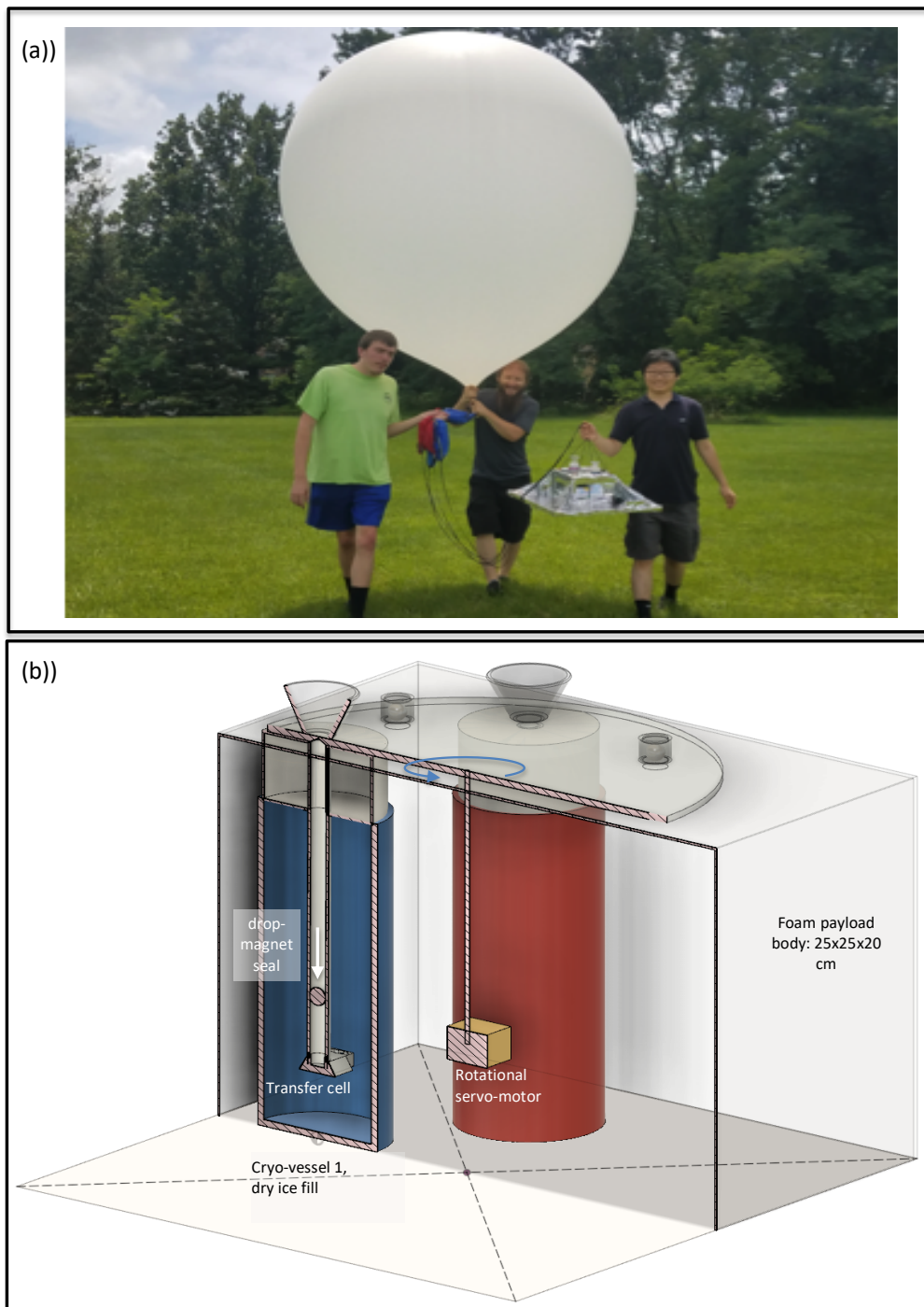
407 **4.4 Composition and morphology of embedded and nucleating aerosol**

408 Cirrus particles also show high variability with respect to the presence of aerosol particulates
409 adhered to the crystal surfaces, and embedded within the sub-surface. In the cleanest cases, most
410 ice particles revealed no obvious (>50 nm radius) non-ice aerosols on the surface (e.g. Fig. 3a),
411 while in the dirtiest cases (Fig. 4a.; Supplement 1D.), each ice particle averaged several dozen
412 mineral or pollutant aerosols. Biogenic particulates are also seen with some frequency (Fig. 5e).
413 While the presence of diverse, rough, complex crystals was striking in every sample collection,
414 the degree of particulate contamination was highly correlated among individual sample
415 collections, suggesting that air-mass-effects play a dominant role in widely-varying degrees of
416 aerosol loading. The opportunity to directly image aerosol particle morphology, relationship to
417 the ice particle surface, and measurement of composition may help to strengthen understanding
418 of connections between aerosol particles, ice nuclei, ice particle growth, and macro-scale cirrus
419 properties.

420



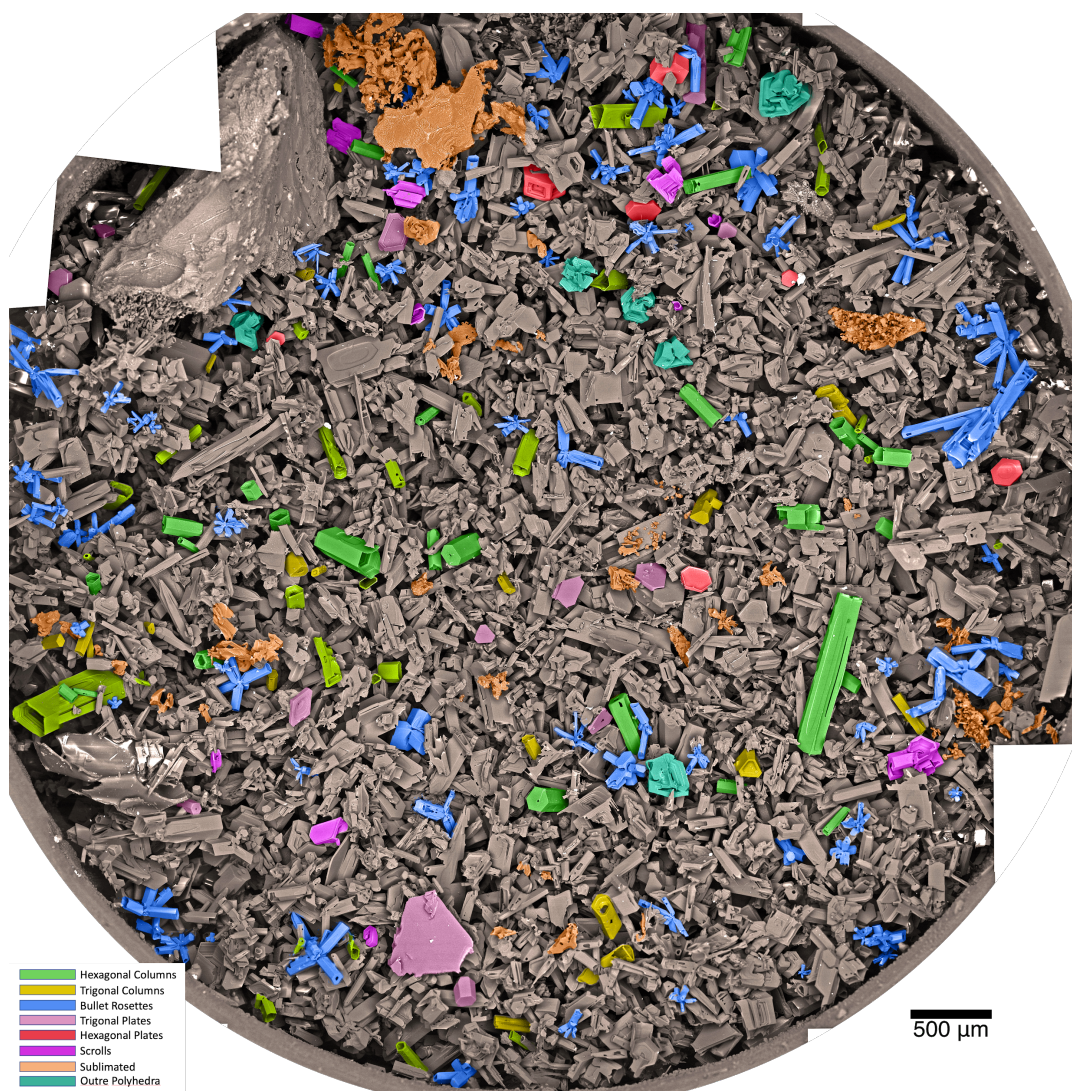
421 **Figure 1.** ICE-Ball balloon and payload photo at pre-launch (a), with co-authors Lynn, Tusay and Zhao
422 (left to right). Diagram of servo-driven sealing of cryo-capture vessels and positioning within the ICE-
423 Ball payload (b).
424
425
426
427
428
429
430





431
432
433
434
435
436
437
438
439

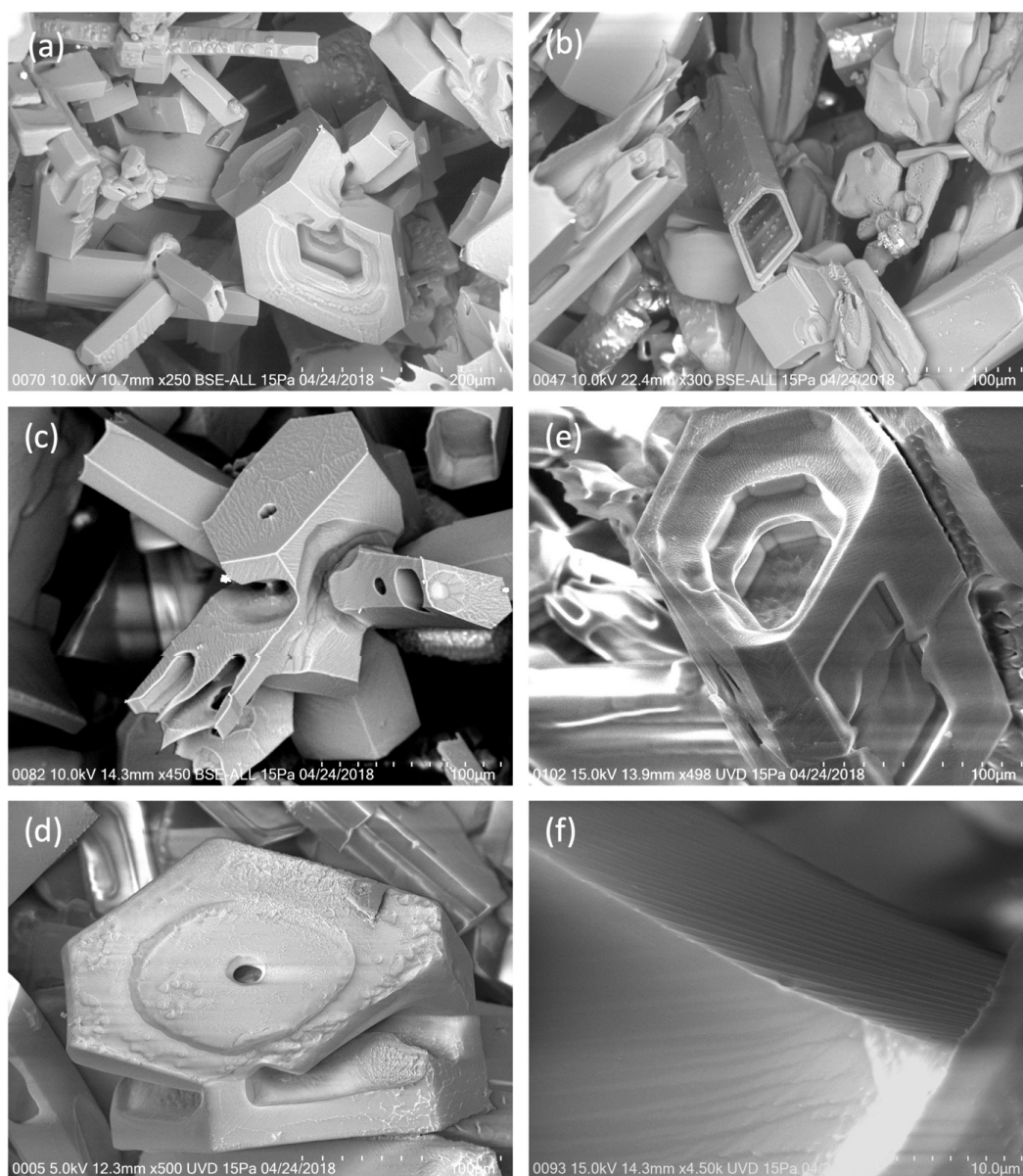
Figure 2. Mosaic of 50 Cryo-SEM micrographs of cirrus ice particles captured on 4/24/2018 from ~11 km altitude, -50°C. Each micrograph in this group was acquired at 100x magnification, with resolution of ~900 nm. Actual large circle diameter 7 mm. False color shading groups similar crystal habits, or highly sublimated particles (orange). Grey-scale particles are sharply-faceted crystals that do not easily fit in habit classification categories. Table 1 provides class counts and geometric measures.



440
441
442
443



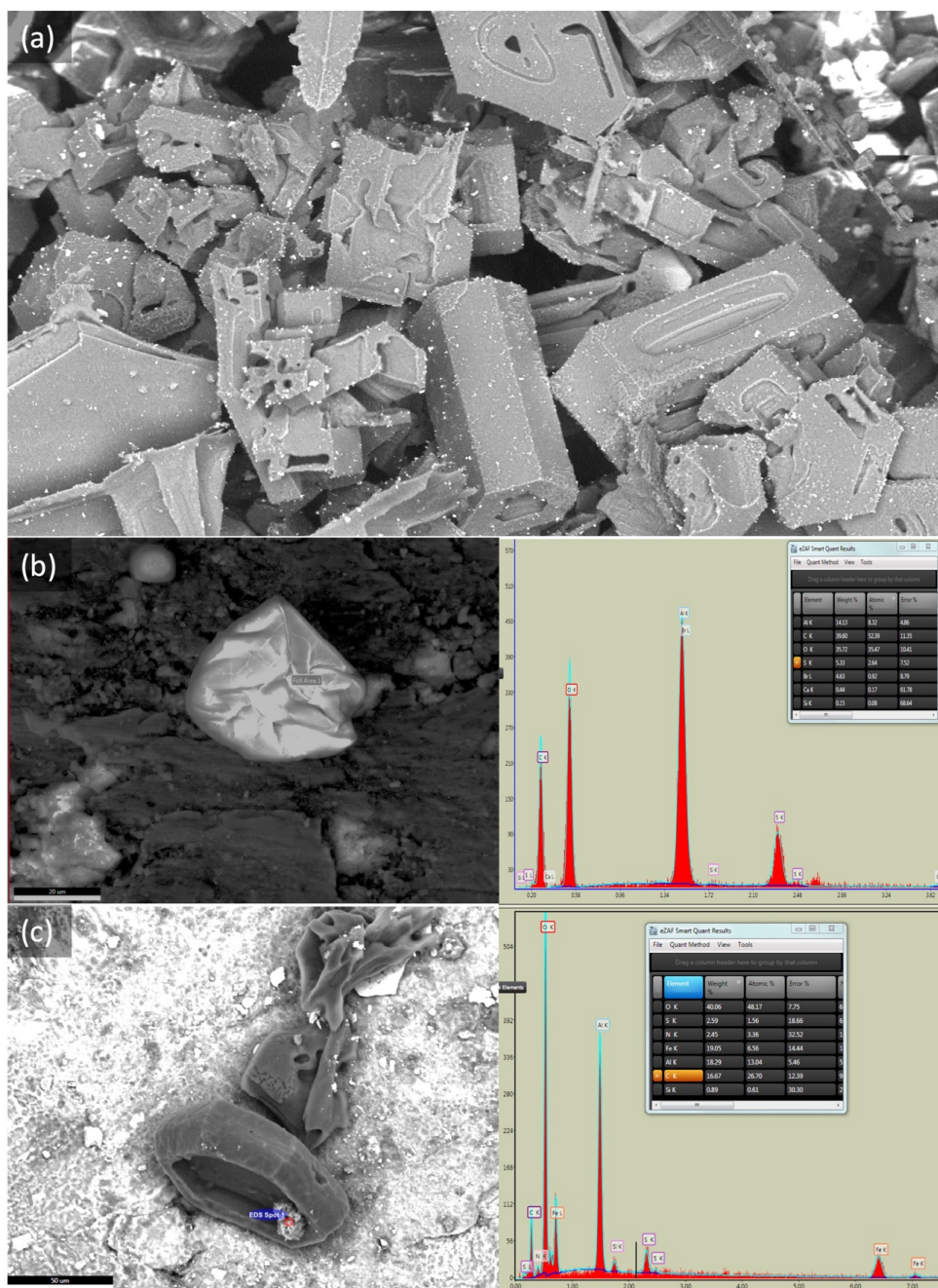
444 **Figure 3.** Moderate magnifications (250x to 4500x) of particles, highlighting a wide variety of surface
445 roughening characteristics. (a) example of a compact-convoluted “outré polyhedron” near several bullet
446 rosettes and non-classified sharp-faceted particles. On close inspection, multiple patterns of roughness
447 visible and several mineral aerosols (bright white). (b) rhomboid column with prismatic linear roughening
448 speckled with discrete surface adhesions, possibly from multiple growth cycles. (c) Rosette with mixed
449 aspect crystals and an array of geometric surface pits and high mesoscopic roughening. (d) Geometrically
450 tiered and hollowed column of irregular basal cross-section with high roughening. (e) Outré polyhedron
451 with central hole and irregular roughening. F. High magnification of small, uniform angular roughening.
452



453



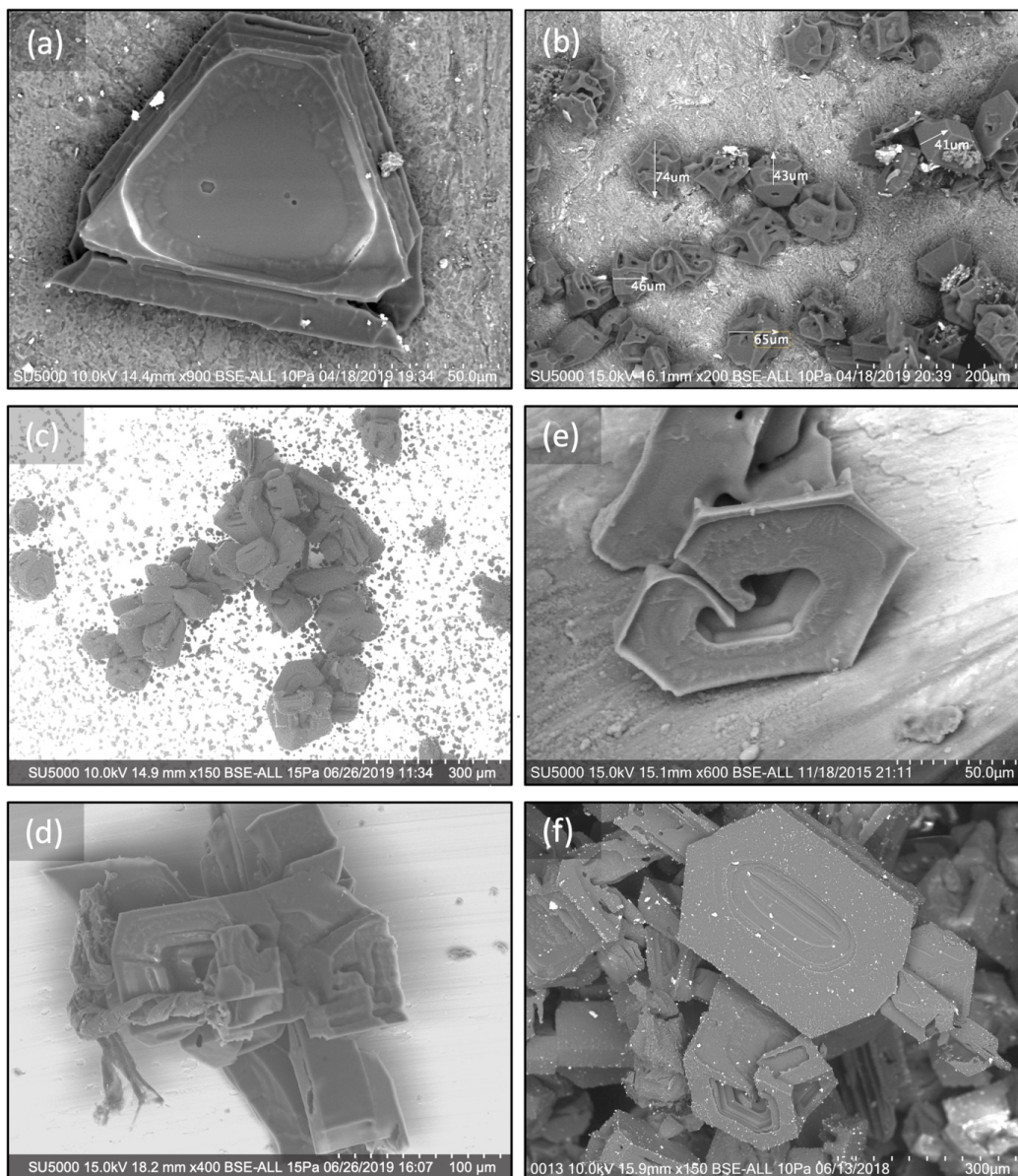
454 **Figure 4.** Three-panel Particle images and Energy Dispersive X-ray Spectroscopy (EDAX Octane)
455 statistics on ice particle contaminants. (a) 100x image of high-aerosol loading on 6/13/2018 (Supplement
456 1D. for additional details). (b) Fly Ash particle (not ice) captured outside cirrus cloud, with EDS
457 composition. (c) Shallow hollowed trigonal ice particle with iron-rich embedded aerosol (6/25/2019).
458



459



460 **Figure 5.** Ice particles with non-classical facet features. A. Trigonal crystal with 3 six-sided etch pits,
461 moderate roughening and aerosol loading. B. Relatively small, compact ice crystals (mean diameter ~55
462 μm) with convoluted hollowing patterns and moderate mineral dust aerosol load. C. Curving chain of a
463 ~15 particle aggregate including rosettes, compact crystals, and outre polyhedra. D. Moderately
464 roughened, scrolled plate with corner fins. E. Complex rosette with twisted biogenic particle (left side). F.
465 Flattened, patterned hexagon with many small adhered aerosols and outre polyhedron (below).
466



467
468
469



470 **Table 1.** Statistics for particle habit categories in Figure 2.
 471

Particle Type	Fig 1. Color	Count	Fit ellipse semi-major mean, μm median	Fit ellipse semi-minor mean, μm median	X-section area mean, μm^2 median Tot. area%	Aspect ratio mean median	Solidity ratio mean median	Note
Columns	Green and Yellow	83	206 167	90 105	18200 10900 4.0%	2.39 2.29	.88 .90	Green columns with hexagonal cross section, yellow non-hexagonal. 90% show hollowing
Bullet Rosettes	Blue	81	189 101	90 57	18800 13400 4.0%	1.84 1.60	.69 .70	Mean of 6 visible bullets per rosette. Bullets range from thick to very thin and solid to hollow.
Highly sublimated	Orange	62	139 93	77 50	18700 3640 3.1%	1.86 1.69	.82 .85	Sublimated to extent original habit and facet shapes not distinguishable.
Plates	Red and Pink	20	218 204	142 125	29300 23800 1.5%	1.64 1.56	.88 .91	Red plates nearly hexagonal; pink are non-hexagonal.
Open Scrolls	Purple	11	183 165	124 80	21100 17900 0.6%	1.51 1.53	.89 .89	Scroll features overlap with other habits; these show dominant scroll features
Outre Polyhedra	Teal	6	250 230	214 193	43000 34200 0.7%	1.17 1.14	.88 .91	Compact particles with convoluted intersecting facets
Complex polycrystals and broken bullets	Gray	~13 00	not measured	not measured	~86%	not measured	not measured	Sharp-faceted polycrystal particles, often of mixed aspect ratio, including broken bullets (10%)

472



Supplementary Files

1. Particle images from additional flights (7-slides)
2. Flight video from 4/18/2018 and flight montage
3. Concurrent map, satellite, and meteorological data for 4/24/2018 (4 slides)

Author Contributions: NM led ICE-Ball development and deployment. KB and SS made major contributions to system development and data analysis. XZ and EK worked extensively on manuscript figures, supplements, and editing. All co-authors participated in multiple field-campaign flight operations, particle acquisition, instrument engineering, and cryo-imaging.

Competing interests: The authors hereby attest they have no competing interests.

Acknowledgements: This work was supported in large part by NSF award 1501096, the TCNJ School of Science and Department of Physics, and student support through NSF award 1557357. The Cryo-SEM facility at TCNJ was made possible by the NJ Building our Future Bond Act. The authors thank TCNJ lab manager Rich Fiorillo for many technical contributions and the Allentown FAA field office for gracious support of balloon launches.



References

- Bailey, M. and Hallett, J.: Growth Rates and Habits of Ice Crystals between -20° and -70°C , *J. Atmos. Sci.* 61, No. 5, 514–554, 2004.
- Bailey, M. P., and Hallett, J.: A comprehensive habit diagram for atmospheric ice crystals: Confirmation from the laboratory, AIRS II, and other field studies. *Journal of the Atmospheric Sciences*, 66(9), 2888-2899, 2009.
- Baran, A. J., Furtado, K., Labonnote, L. C., Havemann, S., Thelen, J. C., and Marengo, F.: On the relationship between the scattering phase function of cirrus and the atmospheric state. *Atmospheric Chemistry and Physics*, 15(2), 1105-1127, 2015.
- Baum, B. A., Yang, P., Heymsfield, A.J., Schmitt, C.G., Xie, Y, Bansemer, A., Hu, Y.,J., Zhang, Z: Improvements in Shortwave Scattering and Absorption Models for the Remote Sensing of Ice Clouds, *J. Appl. Meteor. Climatol.*, 50, 1037–1056, 2011.
- Baumgardner, D., Abel, S.J., Axisa, D., Cotton, R., Crosier, J., Field, P., Gurganus, C., Heymsfield, A., Korolev, A., Kraemer, M. and Lawson, P.: Cloud ice properties: In situ measurement challenges. *Ice Formation and Evolution in Clouds and Precipitation: Measurement and Modeling Challenges*, *Meteor. Monogr.* (58), 2017.
- Burkhardt, U. and Kärcher, B.: Global radiative forcing from contrail cirrus, *Nature Climate Change*, 1, 54–58, 2011.
- Butterfield, N., Rowe, P. M., Stewart, E., Roesel, D., and Neshyba, S.: Quantitative three-dimensional ice roughness from scanning electron microscopy. *Journal of Geophysical Research: Atmospheres*, 122(5), 3023-3041, 2017.
- Cirisan, A., Luo, B. P., Engel, I., Wienhold, F. G., Sprenger, M., Krieger, U. K., Weers, U., Romanens, G., Levrat, G., Jeannet, P., Ruffieux, D., Philipona, R., Calpini, B., Spichtinger, P., and Peter, T.: Balloon-borne match measurements of midlatitude cirrus clouds, *Atmos. Chem. Phys.*, 14, 7341-7365, <https://doi.org/10.5194/acp-14-7341-2014>, 2014.
- Cole, B. H., Yang, P., Baum, B. A., Riedi, J., and C-Labonnote, L.: Ice particle habit and surface roughness derived from PARASOL polarization measurements. *Atmos. Chem. Phys.*, 14(7), 3739-3750, 2014.
- Cziczo, D. J., and Froyd, K. D.: Sampling the composition of cirrus ice residuals. *Atmospheric research*, 142, 15-31., 2014.
- Collier, C. T., Hesse, E., Taylor, L., Ulanowski, Z., Penttilä, A., and Nousiainen, T.: Effects of surface roughness with two scales on light scattering by hexagonal ice crystals large compared to the wavelength: DDA results. *Journal of Quantitative Spectroscopy and Radiative Transfer*, 182, 225-239, 2016.
- Connolly, P., Flynn, M., Ulanowski, Z., Chourolatan, T.W., Gallagher, M., and Bower, K.N.: Calibration of the Cloud Particle Imager Probes Using Calibration Beads and Ice Crystal Analogs: The Depth of Field, *J. Atmos. Oceanic Tech.*, 24, 1860–1879, 2007.
- Fridlind, A.M., Atlas, R., Van Diedenhoven, B., Um, J., McFarquhar, G.M., Ackerman, A.S., Moyer, E.J. and Lawson, R.P.: Derivation of physical and optical properties of mid-latitude



- cirrus ice crystals for a size-resolved cloud microphysics model. *Atmos. Chem. Phys.*, 16(11), 7251, 2016.
- Fugal, J. P., Shaw, R. A., Saw, E. W., and Sergeyev, A. V.: Airborne digital holographic system for cloud particle measurements. *Applied Optics*, 43(32), 5987-5995., 2004.
- Harrington, J. Y., Lamb, D., and Carver, R.: Parameterization of surface kinetic effects for bulk microphysical models: Influences on simulated cirrus dynamics and structure, *J. Geophys. Res.* 114, D06212, 2009.
- Heymsfield, A.J., Krämer, M., Luebke, A., Brown, P., Cziczo, D.J., Franklin, C., Lawson, P., Lohmann, U., McFarquhar, G., Ulanowski, Z. and Van Tricht, K. Cirrus clouds. *Meteorological Monographs*, 58, 2-1, 2017.
- Hioki, S., Yang, P., Baum, B. A., Platnick, S., Meyer, K. G., King, M. D., and Riedi, J.: Degree of ice particle surface roughness inferred from polarimetric observations. *Atmos. Chem. Phys.*, 16(12), 7545-7558, 2016.
- Järvinen, E., Wernli, H., and Schnaiter, M.: Investigations of Mesoscopic Complexity of Small Ice Crystals in Midlatitude Cirrus. *Geophysical Research Letters*, 45(20), 11-465, 2018a.
- Järvinen, E., Jourdan, O., Neubauer, D., Yao, B., Liu, C., Andreae, M. O., and Schnaiter, M.: Additional global climate cooling by clouds due to ice crystal complexity. *Atmos. Chem. Phys.*, 18(21), 15767-15781, 2018b.
- Kärcher, B.: Formation and radiative forcing of contrail cirrus. *Nature Communications*, 9(1), 1824, 2018.
- King, N. J., Bower, K. N., Crosier, J., and Crawford, I.: Evaluating MODIS cloud retrievals with in situ observations from VOCALS-REx, *Atmos. Chem. Phys.*, 13, 191–209, <https://doi.org/10.5194/acp-13-191-2013>, 2013.
- Kuhn, T., and Heymsfield, A. J. : In situ balloon-borne ice particle imaging in high-latitude cirrus. *Pure and Applied Geophysics*, 173(9), 3065-3084, 2016.
- Lawson, R. P., Woods, S., Jensen, E., Erfani, E., Gurganus, C., Gallagher, M., ... and Heymsfield, A. A review of ice particle shapes in cirrus formed in situ and in anvils. *Journal of Geophysical Research: Atmospheres*, 124(17-18), 10049-10090, 2019.
- Magee, N. B., Miller, A., Amaral, M., and Cumiskey, A.: Mesoscopic surface roughness of ice crystals pervasive across a wide range of ice crystal conditions. *Atmos. Chem. Phys.*, 14(22), 12357-12371, 2014
- Mahrt, F., Kilchhofer, K., Marcolli, C., Grönquist, P., David, R.O., Rösch, M., Lohmann, U. and Kanji, Z.A.: The Impact of Cloud Processing on the Ice Nucleation Abilities of Soot Particles at Cirrus Temperatures. *Journal of Geophysical Research: Atmospheres*, 2019.
- Mauno, P., G. M. McFarquhar, P. Räisänen, M. Kahnert, M. S. Timlin, and T. Nousiainen.: The influence of observed cirrus microphysical properties on shortwave radiation: A case study over Oklahoma, *J. Geophys. Res.*, 116, D22208, 2011.
- McFarlane, S. A., and Marchand, R. T. : Analysis of ice crystal habits derived from MISR and MODIS observations over the ARM Southern Great Plains site. *Journal of Geophysical Research: Atmospheres*, 113(D7), 2008.



- Miloshevich, L. M., and Heymsfield, A. J.: A balloon-borne continuous cloud particle replicator for measuring vertical profiles of cloud microphysical properties: Instrument design, performance, and collection efficiency analysis. *Journal of Atmospheric and Oceanic Technology*, 14(4), 753-768, 1997.
- Murray, B. J., Salzmann, C. G., Heymsfield, A. J., Dobbie, S., Neely III, R. R., and Cox, C. J.: Trigonal ice crystals in Earth's atmosphere. *Bulletin of the American Meteorological Society*, 96(9), 1519-1531, 2015.
- Nelson, J., and Swanson, B. D.: Lateral facet growth of ice and snow—Part 1: Observations and applications to secondary habits. *Atmos. Chem. Phys.*, 19(24), 15285-15320, 2019.
- Neshyba, S. P., Lowen, B., Benning, M., Lawson, A., and Rowe, P.M.: Roughness metrics of prismatic facets of ice. *J. Geophys. Res. - Atmos.*, 2013.
- Pfalzgraff, W.C., Hulscher, R.M., and Neshyba, S.P.: Scanning electron microscopy and molecular dynamics of surfaces of growing and ablating hexagonal ice crystals, *Atmos. Chem. Phys.*, 10, 2927-2935, 2010.
- Pratt, K. A., DeMott, P. J., French, J. R., Wang, Z., Westphal, D. L., Heymsfield, A. J., and Prather, K. A.: In situ detection of biological particles in cloud ice-crystals. *Nature Geoscience*, 2(6), 398, 2009.
- Randel, W. J., and Jensen, E. J.: Physical processes in the tropical tropopause layer and their roles in a changing climate. *Nature Geoscience*, 6(3), 169, 2013.
- Saito, M., Iwabuchi, H., Yang, P., Tang, G., King, M. D., and Sekiguchi, M.: Ice particle morphology and microphysical properties of cirrus clouds inferred from combined CALIOP-IIR measurements. *Journal of Geophysical Research: Atmospheres*, 122(8), 4440-4462, 2017.
- Schmitt, C. G., and Heymsfield, A. J.: On the occurrence of hollow bullet rosette—and column-shaped ice crystals in midlatitude cirrus. *Journal of the atmospheric sciences*, 64(12), 4514-4519, 2007.
- Schnaiter, M., Järvinen, E., Ahmed, A., and Leisner, T.: PHIPS-HALO: the airborne particle habit imaging and polar scattering probe—Part 2: Characterization and first results. *Atmospheric Measurement Techniques*, 11(1), 341, 2018.
- Schnaiter, M., Järvinen, E., Vochezer, P., Abdelmonem, A., Wagner, R., Jourdan, O., ... and Ulanowski, Z.: Cloud chamber experiments on the origin of ice crystal complexity in cirrus clouds. *Atmos. Chem. Phys.*, 16(8), 5091-5110., 2016.
- Smith, H. R., Connolly, P. J., Baran, A. J., Hesse, E., Smedley, A. R., and Webb, A. R.: Cloud chamber laboratory investigations into scattering properties of hollow ice particles. *Journal of Quantitative Spectroscopy and Radiative Transfer*, 157, 106-118, 2015.
- Sun, W., Hu, Y., Lin, B., Liu, Z., and Videen, G.: The impact of ice cloud particle microphysics on the uncertainty of ice water content retrievals, *J. Quant. Spectrosc. Ra.*, 112, 189-196, 2011.
- Tang, G., Panetta, R. L., Yang, P., Kattawar, G. W., and Zhai, P. W.: Effects of ice crystal surface roughness and air bubble inclusions on cirrus cloud radiative properties from



- remote sensing perspective. *Journal of Quantitative Spectroscopy and Radiative Transfer*, 195, 119-131, 2017.
- Ulanowski, Z., Hirst, E., Kaye, P. H., and Greenaway, R.: Retrieving the size of particles with rough and complex surfaces from two-dimensional scattering patterns. *Journal of Quantitative Spectroscopy and Radiative Transfer*, 113(18), 2457-2464, 2012.
- Um, J. and McFarquhar, G.M.: Dependence of the single-scattering properties of small ice crystals on idealized shape models, *Atmos. Chem. Phys.*, 11, 3159-3171, 2011.
- Van Diedenhoven, B., Cairns, B., Fridlind, A.M., Ackerman, A.S. and Garrett, T.J.: Remote sensing of ice crystal asymmetry parameter using multi-directional polarization measurements-Part 2: Application to the Research Scanning Polarimeter. *Atmos. Chem. & Phys.*, 13(6), 2013.
- van Diedenhoven, B.: The prevalence of the 22 halo in cirrus clouds. *Journal of Quantitative Spectroscopy and Radiative Transfer*, 146, 475-479, 2014.
- van Diedenhoven, B., Um, J., Mcfarquhar, G. M., and Moyer, E. J.: Derivation of physical and optical properties of midlatitude cirrus ice crystals for a size-resolved cloud microphysics model. *Atmos. Chem. Phys.*, 16, 7251-7283, 2016a.
- van Diedenhoven, B., Ackerman, A. S., Fridlind, A. M., and Cairns, B.: On averaging aspect ratios and distortion parameters over ice crystal population ensembles for estimating effective scattering asymmetry parameters. *Journal of the atmospheric sciences*, 73(2), 775-787, 2016b.
- Voigtländer, J., Chou, C., Bieligk, H., Clauss, T., Hartmann, S., Herenz, P., Niedermeier, D., Ritter, G., Stratmann, F. and Ulanowski, Z.: Surface roughness during depositional growth and sublimation of ice crystals. *Atmos. Chem. Phys.*, 18(18), 13687-13702., 2018.
- Wolf, V., Kuhn, T., Milz, M., Voelger, P., Krämer, M., and Rolf, C.: Arctic ice clouds over northern Sweden: microphysical properties studied with the Balloon-borne Ice Cloud particle Imager B-ICI. *Atmos. Chem. Phys.*, 18(23), 17371-17386, 2018.
- Yang, H., Dobbie, S., Herbert, R., Connolly, P., Gallagher, M., Ghosh, S., and Clayton, J.: The effect of observed vertical structure, habits, and size distributions on the solar radiative properties and cloud evolution of cirrus clouds, *Q. J. Roy. Meteor. Soc.*, 138(666), 1221-1232, 2012.
- Yang, P. and Liou, K.N.: Single-Scattering Properties of Complex Ice Crystals in Terrestrial Atmosphere, *Contr. Atmos. Phys.*, 71, 223-248, 1998.
- Yang, P., Hong, G., Kattawar, G., Minnis, P., and Hu, Y.: Uncertainties Associated with the Surface Texture of Ice Particles in Satellite-Based Retrieval of Cirrus Clouds: Part I -- Single Scattering Properties of Ice Crystals with Surface Roughness, *IEEE Transactions on Geoscience and Remote Sensing*, 46, 1940-1947, 2008.
- Yang, P., Hong, G., Kattawar, G., Minnis, P., and Hu, Y.: Uncertainties Associated With the Surface Texture of Ice Particles in Satellite-Based Retrieval of Cirrus Clouds: Part II-- Effect of Particle Surface Roughness on Retrieved Cloud Optical Thickness and Effective Particle Size, *IEEE Transactions on Geoscience and Remote Sensing*, 46, 1948-1957, 2008.



- Yang, P., Bi, L., Baum, B. A., Liou, K. N., Kattawar, G. W., Mishchenko, M. I., and Cole, B.: Spectrally Consistent Scattering, Absorption, and Polarization Properties of Atmospheric Ice Crystals at Wavelengths from 0.2 to 100 μ m., *J. Atmos. Sci.*, 70(1), 330-347, 2013.
- Yang, Ping, Souichiro Hioki, Masanori Saito, Chia-Pang Kuo, Bryan A. Baum, and Kuo-Nan Liou.: A review of ice cloud optical property models for passive satellite remote sensing. *Atmosphere* 9, no. 12, 499, 2018.
- Yi, B., Yang, P., Liu, Q., Delst, P., Boukabara, S. A., and Weng, F.: Improvements on the ice cloud modeling capabilities of the Community Radiative Transfer Model. *Journal of Geophysical Research: Atmospheres*, 121(22), 2016.
- Yi, B., Yang, P., Baum, B. A., L'Ecuyer, T., Oreopoulos, L., Mlawer, E. J., Heymsfield, A.J. and Liou, K. N: Influence of ice particle surface roughening on the global cloud radiative effect, *J. Atmos. Sci.*, 2013.
- Zhang, Y., Forrister, H., Liu, J., Dibb, J., Anderson, B., Schwarz, J. P., and Nenes, A.: Top-of-atmosphere radiative forcing affected by brown carbon in the upper troposphere. *Nature Geoscience*, 10(7), 486, 2017
- Zhao, B., Wang, Y., Gu, Y., Liou, K. N., Jiang, J. H., Fan, J., and Yung, Y. L.: Ice nucleation by aerosols from anthropogenic pollution. *Nature Geoscience*, 12(8), 602-607, 2019.